Notes on Weightfield2 - Resistive Silicon Detectors

Danush Shekar
Supervised by Dr. Zhenyu Ye

September 20, 2023

Contents

Colour legend

This document will follow a highlighting scheme where text highlighted in different colors mean the following:

Yellow coloured text - Doubts, or sentences that are to be clarified/understood later.
Green coloured text - Some takeaways.
Purple coloured text - Interesting and unique points, that often are not mentioned explicitly in textbooks/literature.

1   About

The WeightField[1] (WF) software is a tool used to simulate a variety of silicon detectors: different versions have been updated over time to study a variety of silicon sensors. As the name suggests, the WeightField2[2] (WF2) software is the second iteration of WF. An important step in detector simulations is the calculation of the electric and weighting fields, and only then the induced current calculations follow. For WF and WF2, the weighting potential is calculated by solving for the Laplace equation using numerical methods (which also involves interpolation), and the induced current is calculated using the Shockley-Ramo theorem.

WF2-RSD (WF2 - Resistive Silicon Detectors) is a version of software that rolled-out after WF2. The primary objective of this tool is to simulate RSDs (or also known as AC-LGADs). In some parts of the code, I believe (and this is a personal opinion) that quantities being calculated are mimicking the experimental results and not truly simulating the physics behind such processes. This might also partly be because we still don't know what is happening in AC-LGADs, for example, the signal induction to the AC pads.

Two references that explain some working principles of WF2-RSD are [2] and [13]. The former discusses the models used to calculate the charge sharing (among different pads) and signal delay and the later is a more detailed article on the same.

WF2-RSD differs from WF2 in the following aspects:

1. Resistive layer - capability to simulate a resistive layer with a user-defined resistivity.

2. Addition of circular pads (instead of strips) by default - User can change number of pads, and packing (square and hexagonal packing of the pads).

3. Naturally, the signal induction calculation has been updated, and the signal sharing model (Logarithmic attenuation model [13]) has also been included.

2   Input Panel Variables/Quantities

The WF2-RSD front-end has many parameters and sections for plots and an example of the same can be seen in Figure 1a. This section walks the reader through what each section is for, along with a brief description of the quantities/results involved.

2.1   Panel: Detector properties

There are 3 detector types under the "**Type**" section (namely Silicon, diamond, and SiC). This refers to the type of material the detector is made of. Each option would involve different values for quanitities like dielectric constant, (e/h) mobilities, etc.

Since we are dealing with AC-LGADs, in the next section "**Doping Type**" would only involve choosing

---

[1]The manual for this (first) version can be found at here
[2]Main link to manuals/guides - http://personalpages.to.infn.it/ cartigli/Weightfield2/Manual.html.

n-type strips (referring to the n+ layer) and p-type bulk.

The options involved with the "**Dimensions**" section and their description are as follows:

1. Stacked - Switching-on this option will go from rectangularly packed pads (default) to hexagonal packing of the pads.

2. Number of pads - The number of pads that will be present in the sensor geometry. A screenshot of the simulation window/screen for 2 different pad numbers are shown in Figure 1.
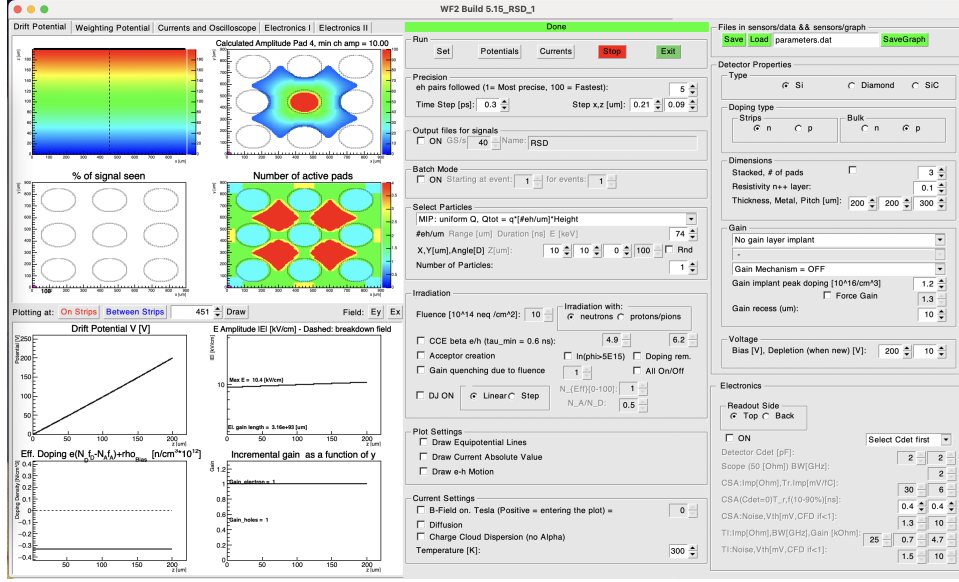
(a)
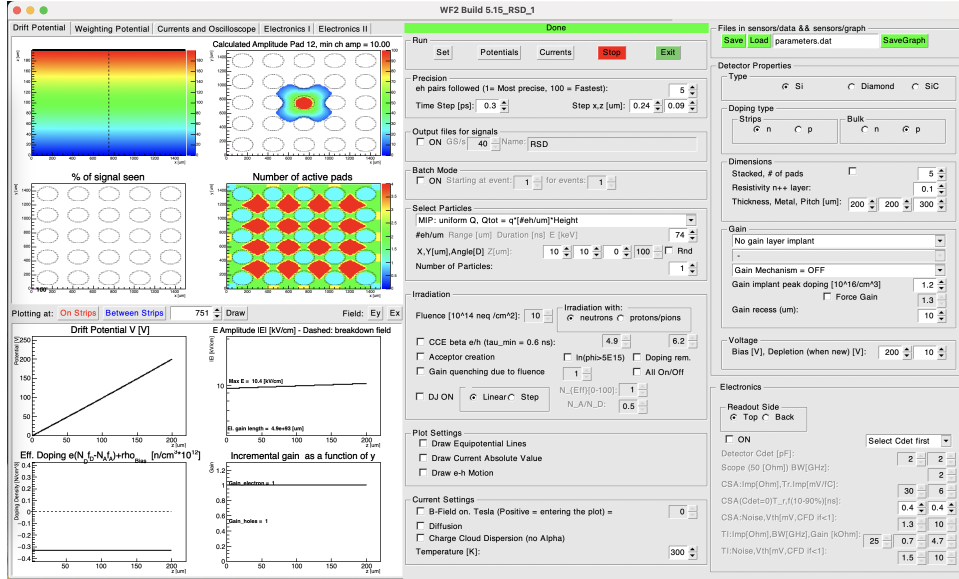
(b)

Figure 1: Software settings and results for (a) 3 × 3 and (b) 5 × 5 pad structures.

3. Resistivity n+ layer - Refers to the resistivity of the n+ layer. The sheet resistance is set to 1kΩ/□. Check for changes in current for different resistivity values.

4. Thickness - The thickness of the detector (if one observes carefully, there is no consideration of pad thickness - which does not affect the potential values under the pads, i.e. in the detector

volume). The value that is assigned to this quantity is the thickness of the bulk substrate (active volume - where the primary charges are created by an incident radiation). The top left plot under drift-potential plots is the cross-sectional plot of the electric potential across the detector.

5. Metal - The diameter of the circular pads (Reference - slide 16).

6. Pitch - The distance between 2 adjacent pads. Should be greater than the metal diameter ofcourse.

The options' description for the "**Gain**" section:

1. Dopant material - Options include Boron, Boron+Carbon, Gallium, and Gallium+Carbon. The addition of Carbon is known to improve radiation hardness [5].

2. Gain layer uniformity+position:

   - Uniform corresponds to a uniform doping concentration.

   - The numbers that follow after the setting/configuration is the position of the electrode from which the gain layer will be implanted.

   - LD corresponds to Low-Diffusion [sensors with, say a Boron gain layer that were exposed to a reduced thermal load during production to minimize the diffusion of Boron (Boron low-diffusion)] [5]. See this link for a better picture.

   - The number that precedes the configuration refers to the identification tag/name given to the sensor version (Eg - 3.1 refers to the HPK-3.1 sensors made by HPK) [7, 8].

   - There is one option with the word 'Epi': it refers to an Epitaxial substrate. Although as the setting suggests that the depth of the layer is 3 μm, but the effective doping plot shows that the layer begins somewhere between 199 μm and 200 μm (a small offset is also present for other implant settings).

3. Forced gain value - According to Cartiglia's website manual, one can forcefully set a gain value, which in-turn removes the dependance from the bias voltage. A hint along the same direction to what is happening with this step can be understood from Figure 10 in[5].

4. Impact-ionization models - Simulation of the gain mechanism through various models. The user has a choice between 4 models, namely, Van Overstraeten model, Okuto-Crowell model, Bologna model, and Massey-LGAD model. Table 2 summarises some differences between these 4 models.

Sensor Version/Name	Thickness	Implant level
HPK-1.2	35μm	Shallow (1.1-1.5μm)
HPK-3.1	50μm	Deep (1.3-1.9μm)
HPK-3.2	50μm	Deeper (1.9-2.3μm)

Table 1: Comparison of some parameters of 3 types of sensors used in WF2-RSD simulations. The numbers in paranthesis in the Implant level column are ones used in WF2-RSD.

An article [1] reports that the gain layer produced in Low Diffusion (LD-narrower layer profile) is more radiation resistant than the High Diffusion (HD) type; (ii) the co-implantation of carbon in the gain layer volume improves by a factor of $\approx$2 the radiation resistance. Another article [5] additionally reports that Gallium doping is less radiation resistant than Boron doping, and that narrower gain layer implants are more radiation resistant than wider implants.

Model	Year Introduced	Valid over:	
		Electric field (x10^5 Vcm^{-1})	Temperature (K)
Van Overstraeten	1970	1.75 - 6.4	NIL
Okuto-Crowell	1975	1.0 - 10.0	Around 300
Massey	2006	2.0 - 8.0	14 - 420
Bologna	1999	0.5 - 6.0	300 - 700

Table 2: Some differences between the impact-ionization models that can be used in WF2-RSD.

2.2 Panel: Electronics

1. Detector capacitance

2. Oscilloscope bandwidth

3. Charge Sensitive Amplifier:

    - Input resistance
    - Rise time/ fall time
    - Trans-Impedance (TI)
    - Noise and threshold voltage

4. Broad-Band Amplifier (referred to as the shaper in the source code):

    - Bandwidth and gain
    - Noise and threshold voltage

For the entirety of this report, unless mentioned otherwise, the legend for the plots from the "Currents and Oscilloscope" tab (which includes and is not limited to the signal from the AC-pads and the oscilloscope) is shown in Figure 2. If there are other colored lines in the plots than what is seen in the figure, that represents the signal seen by the remaining AC-pads as only colors for two AC-pads are shown in the legend.
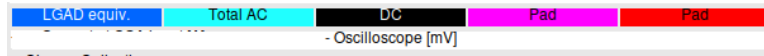

Figure 2: The legend for the plots containing the response of the AC-pads, DC contact, and the oscilloscope (thin-grey line).

Changing parameters of the Charge Sensitive Amplifier (CSA), changes the (Broad-Band) BB amplifier output. This probably suggests that we are looking at a readout 'chain' (sensor → CSA → TI) and not two independent amplifier outputs. Although this is not evident when looking at the code for how these two quantities are calculated.
First, some CAS and TI amplifier parameters were investigated: the noise and threshold voltages (of both CSA and TI) were varied to study what changes they introduce in the final output. A noise voltage of 0.001, 0.1, 1.5, 10, and 50 mV (while other parameters were kept constant) did not show any visible changes in the outputs. The same was done for threshold voltage for 0.001, 0.1, 1, 10, and 50 mV (while other parameters were kept constant) and no visible changes were seen in the output. Understanding how noises are calculated and inculcated into the final output is yet to be done.

2.3 Panel: Select Particles

This subsection has been organised according to the particle type, as each particle type have a different set of options that can be configured. The user has an option to choose from Minimum Ionizing Particles (MIPs), X-Rays, Lasers, and a current pulse.

1. MIPs - User can define the incident position of the MIPs and the number of MIPs. The user can select the type of energy deposition:

   - Uniform/Non-uniform energy deposition - fixes the number of electron-hole pairs deposited per μm.
   - Landau - An energy deposition that follows a Landau distribution. One can also have a MIP passing through the detector from left to right (Edge MIP Landau), instead the default top to bottom.

2. Laser - Options can let the user decide if the laser has to enter the detector from top-down, or down-top, or left-right (Edge)

More details on the same can be found in [3].
Edge-TCT measurements (shooting laser beams left-right) are used to measure the depletion depth for a certain voltage bias [12].

2.4 Panel: Batch mode and output files

Running the simulation on a batch mode essentially repeats one run of the simulation many times. One aspect of the results that is different is the plot from the electronics: a single run will show the waveforms of the CSA and the TI, whereas a batch mode run will produce histograms on resolutions that is yet to be understood.
WF2-RSD provides an option to save the output files, the contents of which were not fully sufficient to produce the figures in Section 4. Thus, the source code was modified to store/save the results in a relevant format.

2.5 Panel: Plots

A brief outline of the plots made in the "**Drift Potential**" section is as follows:

1. XZ potential contour (top left) - Contour plot of electric potential across the XZ plane for a Y-plane. Apparently, since we have uniform doping and a uniform active region, this plot should be similar for all Y-values.

2. Calculated amplitude plot (top right) for say, pad 'A' and minimum charge amplitude = say 'B' - Plot across the XY plane that signifies when a particle/radiation passes through a point in that XY-plane, how much of the amplitude reached pad 'A'. Signal amplitude below 'B' is not considered.

3. % of signal seen (bottom left) - For the incident particle(s)/radiation incident at the given position (marked with a purple dot in plot), the percentage amount of the signal reaching nearby pads is represented in this plot. Do **note** that the percentage value is shown below the pad, and not above it. Sometimes two numbers are displayed outside the plot-area, just poor formatting.

4. Number of active pads (bottom right) - A plot on the XY-play, such that, for incoming particle(s)/radiation on a certain point in the plot, how many pads will pick up the signal (this number is given by the z-colour-axis).

3 Brief review of the source code

A few sections of code that are important to know were understood and the same have been described in the following sub-sections. These sub-sections will be updated as more sections of the source code is decoded/interpreted.

3.1 Charge and current generation

Every electron/hole generated, an C++ object (from class `Carriers`)is created that contains information like charge, position, velocity, etc. Most of the charge-generation and current-calculations are done in the file Carriers.cxx. As mentioned in Section 2.3, depending on the charge deposition mechanism the user chooses, an array called `NPairsPer5Micron` is updated with the number of primary charges per 5 μm in the sensor active volume, and objects of the `Carriers` class are created with position and charge information. There is a limit on the number of charges WF2 can track because there is a (large) fixed number of objects defined.

Mobilities are defined and at each time-step, for each particle, the velocities and positions are updated (using the electric field and mobility values). The positions involve both updated from a diffusion and drift component. Then a temporary induced current value is updated based off of this movement for each charge that is calculated using Ramo's theorem. If the charge(s) is in the gain layer region, the user-defined gain model is used and new objects are added to the `Carriers` accordingly. One of the snippets that shows the calculation of the temporary current using Ramo's theorem from electrons (`ie[]`) and holes (`ih[]`) is shown below:

```
    if (carriers[j].GetCharge()==-1)
        ie[i]+=(-1)*(-1)*chargescale*ECHARGE*(wfield[PosBiny][PosBinx].GetFieldx()*
            ↪ carriers[j].GetVx() + wfield[PosBiny][PosBinx].GetFieldy()*carriers[j].
            ↪ GetVy());
        else
                ih[i]+=(-1)*chargescale*ECHARGE*(wfield[PosBiny][PosBinx].GetFieldx()*
                    ↪ carriers[j].GetVx()+ wfield[PosBiny][PosBinx].GetFieldy()*carriers
                    ↪ [j].GetVy());
```

After this, the final current is calculated through a convolution of the (temporary) induced current and an exponential function (kernel). The snippet of code that does the same is as shown below:

```
    for (int i=0;i<IMax-1;i++) //AC discharge
        {
            for (int ll = 0; ll<IMaxSh-i;ll++) // valid only up to IMaxSh
            {
                    CurrentStep = itot[i]*TIMEUNIT/(tau_RSD)*TMath::Exp(-ll*TIMEUNIT/(
                        ↪ tau_RSD));
                    itotQ[i+ll] += -CurrentStep; //final current from the AC pads
                    iDC[i+ll] += CurrentStep; // The current for DC contact
            }
        }
```

The variable `tau_RSD` involves the resistance and capcitance of the n+ layer and the oxide layer respectively.

The output of the oscilloscope, trans-impedance(/broad-band) amplifier, and the charge-sensitive amplifier (/shaper) can be summarised by the following snippet:

```
    for (int ll = 0; ll<IMaxSh-i;ll+=Step) // valid only up to IMaxSh
    {
```

```
Iout_C50[i+ll] += (Qdif_Shaper)/tau_scope*TMath::Exp(-ll*TIMEUNIT/tau_scope);
    ↪ //Qdif_shaper is essentially the charge from the total induced current
Iout_BB_RC[i+ll] += (Qdif_Shaper)/tau_BBA*TMath::Exp(-ll*TIMEUNIT/tau_BBA); //
    ↪ Input current to the BBA, convolution with BW

Vout_scope[i+ll] = 50*Iout_C50[i+ll]; // Output Voltage Scope
BBGraph[i+ll] = 1e+3*BBGain*Iout_BB_RC[i+ll]; // Output Voltage BBA

// saturation of pre-amp output
if ( fabs(BBGraph[i+ll])>800) BBGraph[i+ll] = 800*BBGraph[i+ll]/fabs(BBGraph[i+
    ↪ ll]);
//
if (! gui->GetNA62On())
    {
    ShaperOut_Q[i+ll] += TauFall/(TauFall+TauRise_CSA)*Qdif_Shaper*(TMath::Exp(-
        ↪ ll*TIMEUNIT/TauFall)-TMath::Exp(-ll*TIMEUNIT/TauRise_CSA)); // [Q] HS
        ↪  eq 4.3 This is the shaper
    }
}
```

Ofcourse, there are some further improvisations that we will not get into, for examples, a finite linear interpolation that is done to the voltage outputs of the oscilloscope and amplifiers, there are further plots produced from these quantities, etc.

3.2 Signal sharing model(s)

Signal-sharing is a unique feature that AC-LGADs display and WF2-RSD simulates this effect by using the LOGarithmic-Attenuation (logA) model. The details of this model can be found in [13] alongwith another model that is discussed in the paper: LINear-Attenuation (linA) model. The linA model contains parameters (dependant on the geometry) that has to be experimentally determined and this is why WF2-RSD cannot use this model for signal-sharing simulations. The logA model however can derive the signal-sharing fractions without the need for experimental data. The only limiting factor is that the validity of this model was verified upto distances of 400-500 μm in [13]. The logA model empirically-argues that the signal-sharing fraction is governed by the following equation:

$$F_i\left(\alpha_i, d_i\right) = \frac{\frac{\alpha_i}{\ln(d_i/d_0)}}{\sum_1^n \frac{\alpha_i}{\ln(d_i/d_0)}} \tag{1}$$

where F_i is the fraction of the total signal amplitude seen on the pad i, d_i the distance from the hit point to the pad i metal edge, and α_i the pad i angle of view. [13] also goes on to state that this equation predicts without any free parameter how a signal is shared among pads for every RSD geometry, n^+ resistivity, and dielectric thickness, as the signal sharing depends on the relative resistance of each path, and not on its absolute value.

Once WF2-RSD calculates the total signal induced (which is found through the use of the Ramo's theorem and a convolution), the signals induced in each pad are just this fraction multiplied with the total signal.

4 Reductionist studies of input parameters

WF2-RSD utilises numerous user-defined parameters that have a broad range of effects on the final results. The following sub-sections will describe the (reductionist) study performed on some of these parameters

and the results obtained thereafter. By default, the word 'signal' would be used to refer to the AC pad signal in the following sub-sections.

4.1 n+ layer's resistivity

The dependance of the signal characteristic and gain on the resistivity of the n+ layer was studied, and specifically, if there were any changes to the depletion of the n+ layer ([6] states that doing so changes how much the n+ layer gets depleted).

Results obtained show that increasing the resistivity corresponded to the broadening of the signal's tail on the second lobe and the relevant figures for the same can be seen in Figure 3. The integral of the AC pad signal is known to be 0 (involves a charging and discharging cycle [13]), and the RC value changes for different resistivities, which imply that a change in resistivity value will correspond to a change in the signal shape. However, a conclusive statement for the effect of resistivity on the gain value could not be made using WF2-RSD, atleast not for the values of resistivity that was used for the study.
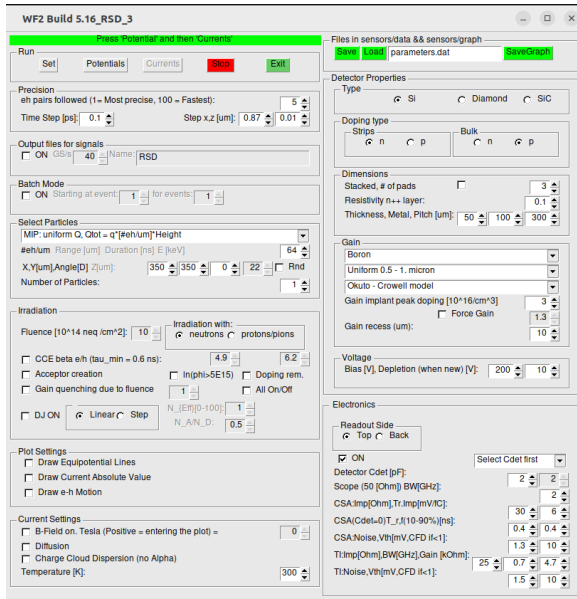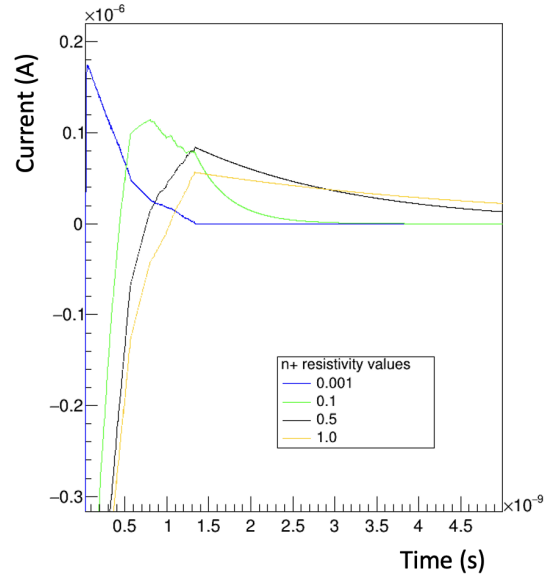
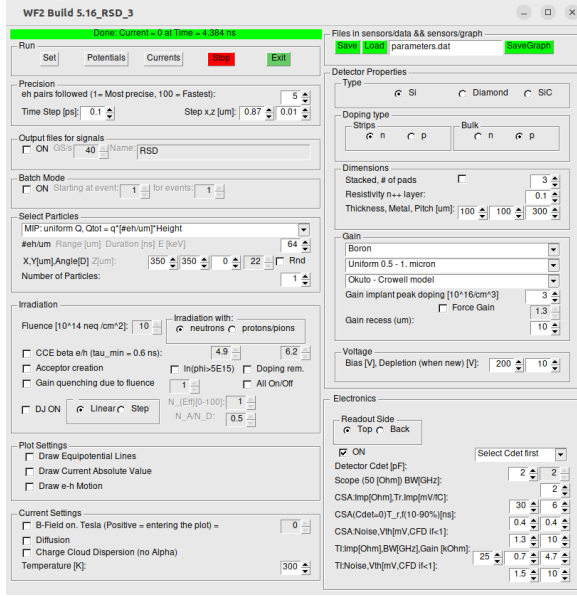(a)   (b)

Figure 3: (a) An image of the settings used for the study and (b) the plot of the compiled results obtained as part of this study. As seen, four different values of n+ resistivity was used: 0.001, 0.1, 0.5, and 1.

Another point to note is that WF2-RSD produced a non-intuitive result for resistivity value = 0.0001. The positive lobe of the signal had a much larger amplitude than those of the other resistivity values.
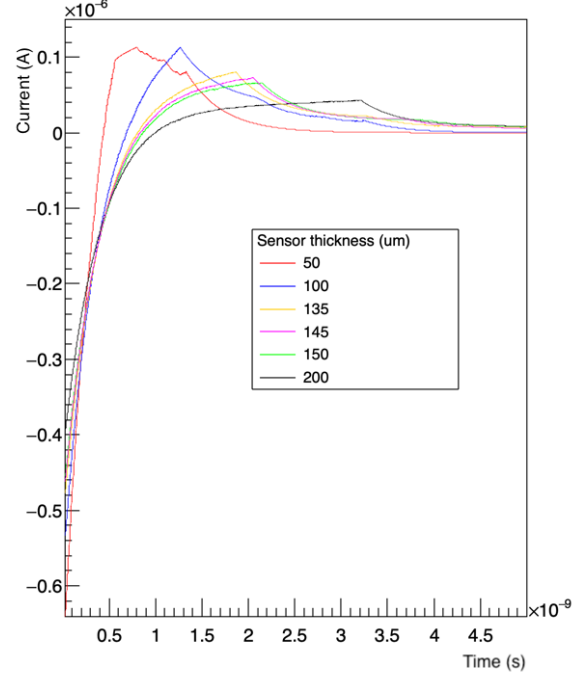
4.2 Thickness

Amongst the early silicon sensors (that had no gain layer), the thickness did not affect the amplitude of the signal because of two factors contributing to this property: the number of initial charges produced is proportional to the thickness, and the weighting field is inversely proportional to the thickness. In AC-LGADs however, things are not so simple. The simulation results showed that the amplitude/height of the first lobe is inversely proportional to the thickness. That said, the first lobe of the signal broadens for thicker detectors which is expected as the holes generated in the active volume will need longer time to traverse a larger distance.

This study was done for thicknesses in steps of 50 μm, but the reason for looking at 135 μm and 145 μm is that alongwith thickness, there was a parallel study on the maximum electric field's variation

Figure 4: (a) An image of the settings used for the study and (b) the plot of the compiled results obtained as part of this study. As seen, four different values of thicknesses was used: 50, 100, 135, 145, 150, and 200 μm.

with thickness. A numerical fluctuation-like effect (probably due to mesh-effects) was observed for the maximum field value around thickness = 150 μm. The corresponding plot is shown below in Figure 5

4.3 Pitch

The currents seen by the AC-pads for different pitches (and simultaneously maintaining the incident position of the charged particle to be at the center of 4 pads always) was simulated. As expected, the signals seen by four closest pads were the same as the sharing fraction remains the same. The motive of this study (and this was just a shot in the dark owing to the unlikeliness of the desired result) was to reach a limit where the resistance is of a lesser impedance value than that of the capacitive oxide. Reaching this limit would have implied all current goes to the DC contact and would not have any current going through the AC pads, and for the values the simulations were performed over, this limit was not reached. However, the results obtained still are as expected in that the signal sharing fractions would not change for the four nearby pads because the incident particle is in the middle of the four pads. Some images form this study are shown in Figure 6. This study was performed for pitches = 220, 300, 350 and 400 μm, and 220 μm instead of 200 μm was chosen because the pad diameter was set as 200 μm.

4.4 Time delay from hit position

Depending on where the incident particle hits the sensor, the signal takes a finite non-zero time taken to reach the electronics. This arises due to the time needed by the charges to reach the electrode, or more specifically, the wirebond. In a centimeter-scale AC-LGAD paper [11], it was reported that for farther hit positions on the strip from the wirebond, the time delay increases. Simulations were done
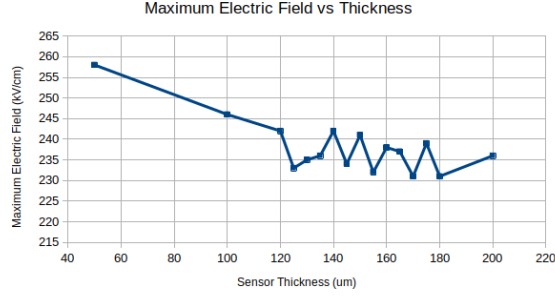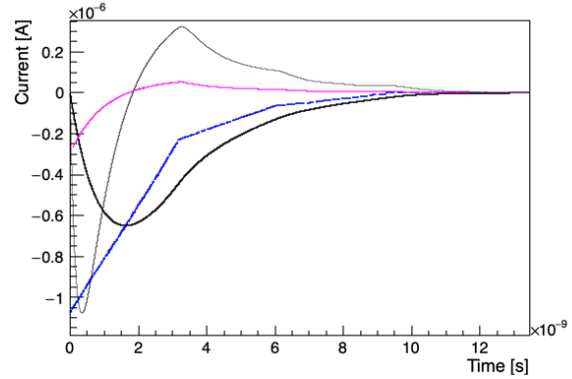
Figure 5: A plot of maximum electric field observed in the sensor for different thicknesses.

Figure 6: (a) An image of the settings used for the study and (b) the electronic response plot for one of the pitch (=300 μm) values considered.

for pad diameters (200, 300, 400, and 450 μm) and varying y-coordinates (100, 150, 200, 250, and 600 μm) for the same x-coordinate (20μm away from the end of the pad). Although the terminal prints a number for the delay, this is calculated by the LogA model for signal sharing and the objective of this study was to observe the physics simulation to naturally introduce time delays in waveforms for AC pads of different dimensions. This time delay would be arising from the non-zero time taken by the charges travelling through the electrode to reach the wirebond. In WF2-RSD, the current and electronic response of a sensor was simulated for different hit positions (in the gap region). A conclusive correlation between this time-delay and distance from the center of the pads to the incident position, was not found. This statement could atleast be made only for the geometries that was tried. It could be the case that the strips displaying this behavior in the above stated paper were of larger order of lengths, hence this effect might not be prominent in smaller pad sizes. The source code also does not have scope to perform this calculations for this kind of a mechanism.

4.5   Coupling capacitance: pad size

There are two ways to vary coupling capacitance: varying the diameter of the pads (on the front panel (GUI) of the software) and by varying the oxide layer thickness. Changing geometry is known to introduce
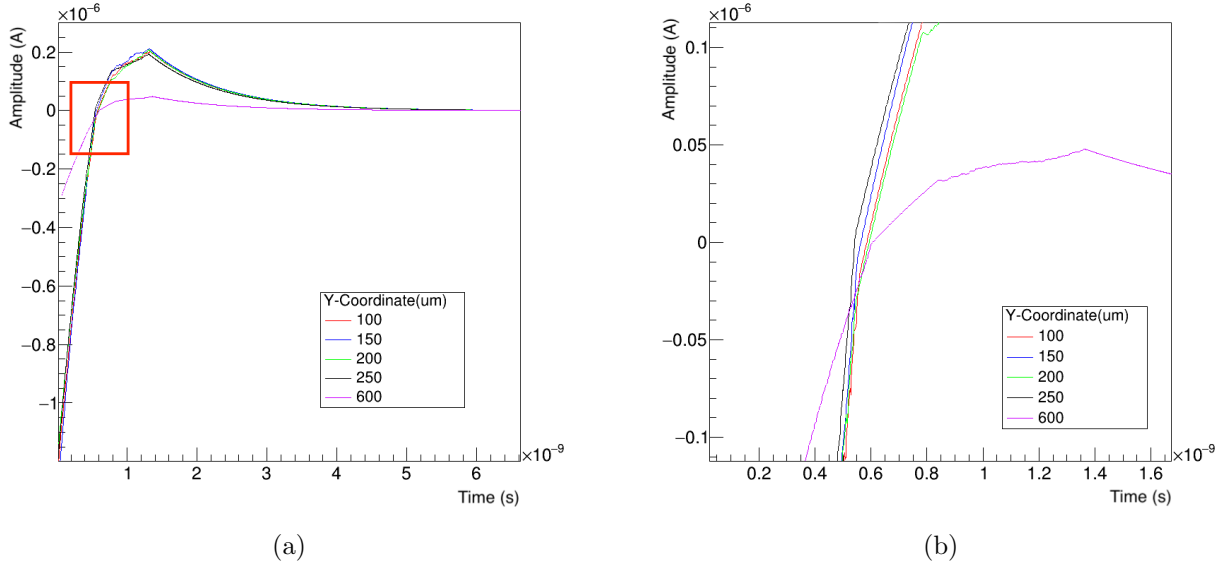
Figure 7: A plot of the signals from a sensor with 50 um thickness, 500 um pitch, 200 um pad width for different incident hit positions (same x-coordinate, but different y-coordinates) in the gap region. The red box in Figure (a) corresponds to the region enlarged to produce Figure (b)).

other effects like inter-strip capacitance so the former method wouldn't be a proper reductionist study. The details of the second way to vary coupling capacitance (by varying the thickness of the oxide layer) will be discussed in Section 4.6. The results of this study are shown in Figure 8. We see that smaller pads offer a path of greater impedance so more current reached the DC terminal than the AC pads. Another inference from Figure 8 is that since smaller pads have smaller capacitance, the tails of the second lobe will also have be smaller.
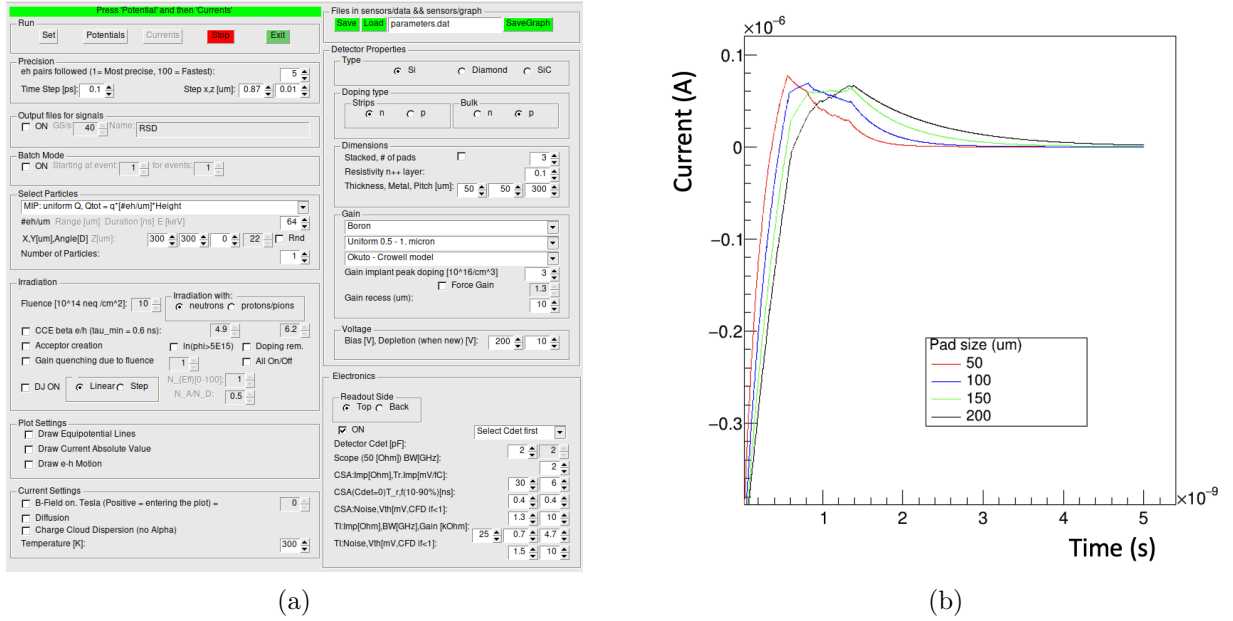

Figure 8: (a) An image of the settings used for the study and (b) the plot of the compiled results obtained as part of this study. As seen, four different values of pad diameters was used: 50, 100, 150, and 200 μm.

4.6 Coupling capacitance: capacitance/area of oxide layer - an attempt to reproduce experimental results

An article [9] reported results on the dependence of signal amplitude for different capacitances for pixel-electrode AC-LGADs. For this study, a sensor of pitch 150 μm and square pad of width 140 μm was used and the subsequent plot the authors obtained is shown in Figure 9.
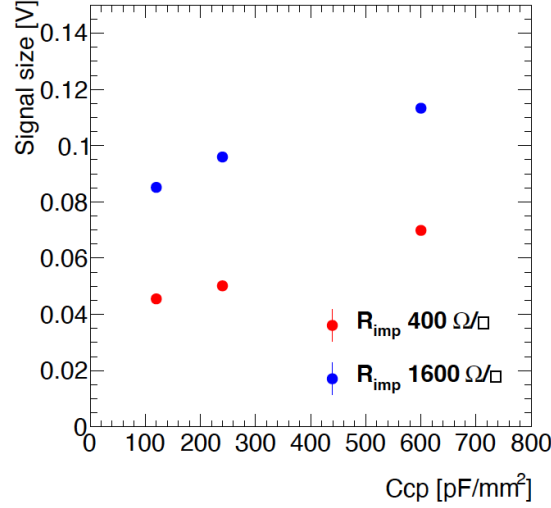

Figure 9: The signal size evaluated using ^{90}Sr as a function of C_{cp}. Each colored point corresponds to fixed sheet resistance value. Source: [9]

As mentioned earlier, a way to change the coupling capacitance without changing the electrode geometry is by varying the oxide layer thickness, which translates to changing the capacitance/area value of the oxide layer in the source code. Using the similar parameter values used in the article, an attempt was made to recreate the same plot using WF2-RSD. The only unknown was the doping concentration of the gain layer, which was not mentioned in the paper, thus this quanitity was set to close to WF2-RSD's default value. The settings used and the results thus obtained is shown in Figure 10. It is worth mentioning that for this study, 100 events were simulated in the batch mode, and each event had one MIP traversing through the detector depositing charge according to a Landau distribution.

The documentation for the simulation tool is not present for the RSD version of WF2 but we believe that the variable named `rsdc1` (that is brought up in calculating the time constants (RC)) found in the Carriers.cxx file is related to the capacitance/area quantity. The signal size (from the AC pads) for different values of `rsdc1` was simulated and the plot thus obtained is shown in Figure 10.
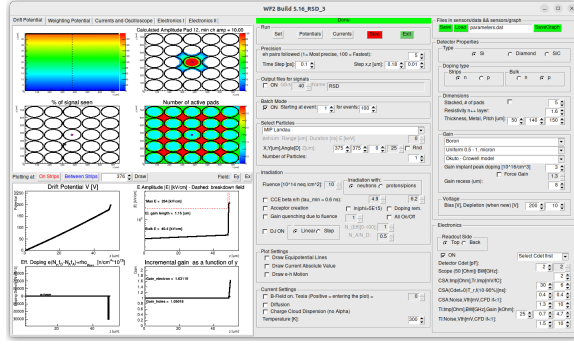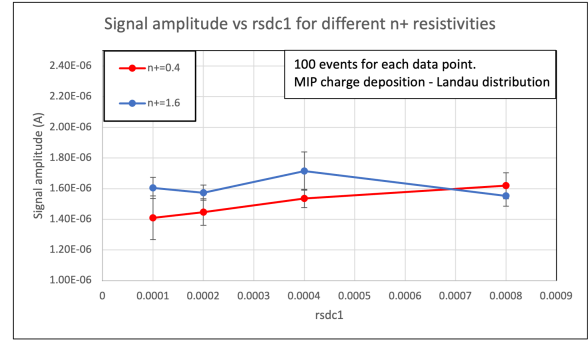
(a)   (b)

Figure 10: (a) An image of the settings used for the study and (b) the plot of the compiled results obtained as part of this study. The X-axis (rsdc1) is the variable in the source code that corresponds to the capacitance/area. Example: an rsdc1 value of 0.0002 = 200pF/mm². The two colored curves correspond to two different sheet resistances (0.4≡400Ω/□ and 1.6≡1600Ω/□).

A Electronics - frequency response

Before delving into the details of some common concepts of electronic response let us walk through two common terminologies used: decibel and bandwidth (in context of oscilloscopes).

A decibel is a relative unit of measurement and when we say the amplitude has changed by a factor of 3 dB, this implies the amplitude has changed by a factor of $\sqrt{2}$. Note that decibel can also be used in context of change in power, in which case 3 dB can mean a change-factor of 2.

An oscilloscope typically will have a bandwidth specified and it is usually the 3dB bandwidth (the meaning will be explained soon). Let us explain what this means through an example: An oscilloscope with bandwidth = 1 GHz implies that a sine wave with frequency above 1 GHz will have it's amplitude degraded by more than 3 dB. Trying to look at a signal that is too fast for a scope's bandwidth will introduce errors in amplitude and/or time-interval measurements. [4].

For a unit step voltage as the input, an oscilloscope will have a corrseponding response: it would take a non-zero time for the output to go from 10 - 90% of the steady state value and this is given by $2.2 \times \tau$. Let us look at how this equation is obtained:

The frequency response of an oscilloscope is closely similar to that of the 1st order, RC low-pass filter [10]. A device with a bandwidth essentially drops out components of the input with a frequency above the bandwidth, similar to that of a low-pass filter. The relationship between the output voltage and the input voltage for a low-pass filter is well known to be:

$$V_{out} = V_{in}\left(1 - \exp\left(-\frac{t}{\tau}\right)\right) \tag{2}$$

where τ = RC, R and C being the resistance and capacitance used to make the low-pass filter. If at t_1, the signal reaches 10% of it's amplitude and at a later time t_2 the signal reached 90% of it's amplitude, we use Equation 2 and with a little manipulation, we obtain:

$$t_1 = -\tau ln(0.9)$$
$$t_2 = -\tau ln(0.1)$$

$$\Rightarrow t_2 - t_1 \equiv T_r = \tau ln(9) \tag{3}$$

We also know (in the frequeny-domain) that the cut-off frequency is given by:

$$\omega = 2\pi f = \frac{1}{RC}$$

Thus we have:

$$\tau = \frac{1}{2\pi f} = \frac{1}{2\pi B} \tag{4}$$

where B is the bandwidth. Then combining results from Equation 2 and 4, we obtain:

$$T_r = \frac{0.35}{2.2 \times B} \tag{5}$$

References

[1] R. Arcidiacono, G. Borghi, M. Boscardin, N. Cartiglia, M. Costa, G.F. Dalla Betta, F. Fausti, M. Ferrero, F. Ficorella, M. Mandurrino, S.M. Mazza, E.J. Olave, L. Pancheri, G. Paternoster, H.-F.W. Sadrozinski, V. Sola, A. Staiano, A. Seiden, F. Siviero, M. Tornago, and Y. Zhao. State-of-the-art and evolution of ufsd sensors design at fbk. *Nuclear Instruments and Methods in Physics Research Section A: Accelerators, Spectrometers, Detectors and Associated Equipment*, 978:164375, 2020.

[2] Nicolo Cartiglia. Innovative silicon sensors for future trackers - Part 2, June 2020.

[3] Francesca Cenna, N. Cartiglia, M. Friedl, B. Kolbinger, H.F.-W. Sadrozinski, A. Seiden, Andriy Zatserklyaniy, and Anton Zatserklyaniy. Weightfield2: A fast simulator for silicon and diamond solid state detector. *Nuclear Instruments and Methods in Physics Research Section A: Accelerators, Spectrometers, Detectors and Associated Equipment*, 796:149–153, 2015. Proceedings of the 10th International Conference on Radiation Effects on Semiconductor Materials Detectors and Devices.

[4] Hewlett Packard Company. Test & Measurement Catalog, 1999.

[5] M. Ferrero, R. Arcidiacono, M. Barozzi, M. Boscardin, N. Cartiglia, G.F. Dalla Betta, Z. Galloway, M. Mandurrino, S. Mazza, G. Paternoster, F. Ficorella, L. Pancheri, H-F W. Sadrozinski, F. Siviero, V. Sola, A. Staiano, A. Seiden, M. Tornago, and Y. Zhao. Radiation resistant lgad design. *Nuclear Instruments and Methods in Physics Research Section A: Accelerators, Spectrometers, Detectors and Associated Equipment*, 919:16–26, 2019.

[6] Gabriele Giacomini. Fabrication of Silicon Sensors Based on Low-Gain Avalanche Diodes. *Frontiers in Physics*, 9, 2021.

[7] M. Jadhav, W. Armstrong, I. Cloet, S. Joosten, S.M. Mazza, J. Metcalfe, Z.-E. Meziani, H.F.-W. Sadrozinski, B. Schumm, and A. Seiden. Picosecond timing resolution measurements of low gain avalanche detectors with a 120 gev proton beam for the topside detector concept. *Journal of Instrumentation*, 16(06):P06008, jun 2021.

[8] Y. Jin, H. Ren, S. Christie, Z. Galloway, C. Gee, C. Labitan, M. Lockerby, F. Martinez-McKinney, S.M. Mazza, R. Padilla, H.F.-W. Sadrozinski, B. Schumm, A. Seiden, M. Wilder, W. Wyatt, Y. Zhao, R. Arcidiacono, N. Cartiglia, M. Ferrero, M. Mandurrino, F. Siviero, V. Sola, M. Tornago, V. Cindro, A. Howard, G. Kramberger, I. Mandić, and M. Mikuž. Experimental study of acceptor removal in ufsd. *Nuclear Instruments and Methods in Physics Research Section A: Accelerators, Spectrometers, Detectors and Associated Equipment*, 983:164611, 2020.

[9] Sayuka Kita, Koji Nakamura, Tomoka Imamura, Ikumi Goya, and Kazuhiko Hara. Development of ac-lgad detector with finer pitch electrodes for high energy physics experiments, 2023.

[10] Thor Labs. Relationship Between Rise Time and Bandwidth for a Low-Pass System.

[11] C. Madrid, R. Heller, C. San Martí n, S. Nanda, A. Apresyan, W.K. Brooks, W. Chen, G. Giacomini, O. Kamer Köseyan, S. Los, C. Peña, R. Rios, A. Tricoli, S. Xie, and Z. Ye. First survey of centimeter-scale AC-LGAD strip sensors with a 120 GeV proton beam. *Journal of Instrumentation*, 18(06):P06013, jun 2023.

[12] Michael Moll. Acceptor removal - Displacement damage effects involving the shallow acceptor doping of p-type silicon devices. *PoS*, Vertex2019:027, 2020.

[13] M. Tornago, R. Arcidiacono, N. Cartiglia, M. Costa, M. Ferrero, M. Mandurrino, F. Siviero, V. Sola, A. Staiano, A. Apresyan, K. Di Petrillo, R. Heller, S. Los, G. Borghi, M. Boscardin, G.-F. Dalla Betta, F. Ficorella, L. Pancheri, G. Paternoster, H. Sadrozinski, and A. Seiden. Resistive ac-coupled silicon detectors: Principles of operation and first results from a combined analysis of beam test and laser data. *Nuclear Instruments and Methods in Physics Research Section A: Accelerators, Spectrometers, Detectors and Associated Equipment*, 1003:165319, jul 2021.